Identification of dislocations in large tetragonal hen egg-white lysozyme crystals by synchrotron white-beam topography

M. Tachibana,[a]* H. Koizumi,[a] K. Izumi,[b] K. Kajiwara[b] and K. Kojima[a]

[a]Graduate School of Integrated Science, Yokohama City University, 22-2 Seto, Kanazawa-ku, Yokohama 236-0027, Japan, and [b]SPring-8/Japan Synchrotron Radiation Research Institute (JASRI), 1-1 Koto, Mikazuki-cho, Sayo-gun, Hyogo 679-5198, Japan. E-mail: tachiban@yokohama-cu.ac.jp

Large tetragonal hen egg-white (HEW) lysozyme crystals have been grown by a salt concentration-gradient method. The grown crystals, of thicknesses greater than 1.5 mm, were observed by means of X-ray topography using white-beam synchrotron radiation. Line contrasts clearly appeared on the Laue topographs. Extinction of the line images was observed in specific reflections. These results mean that the observed lines correspond to dislocation images. From the extinction criterion it is shown that the predominant dislocations are of screw character with ⟨110⟩ Burgers vectors. In addition, dislocation loops with [001] Burgers vectors have been found in a tetragonal HEW lysozyme crystal including some cracks. These results are discussed in the light of dislocation elastic energy and slip systems in the crystals.

Keywords: X-ray topography; protein crystals; crystal defects; dislocations; lysozyme.

1. Introduction

The characterization of crystal defects, especially dislocations, in protein crystals is important for an understanding of their crystallization. The crystallization originating from dislocations has been investigated by means of atomic force microscopy (AFM) (Durbin *et al.*, 1993; Konnert *et al.*, 1994; Malkin *et al.*, 1999; McPherson *et al.*, 2001). However, AFM is limited to local observation of the crystal surface. It is desired that the distribution of dislocations in the whole crystal be observed.

X-ray topography is one of the most powerful methods not only for mapping but also for characterization of dislocations in the whole crystal (Tanner, 1976; Klapper, 1991; Bowen & Tanner, 1998). The application of X-ray topography to protein crystals has been carried out by various groups (Izumi *et al.*, 1996, 1999; Stojanoff & Siddons, 1996; Stojanoff *et al.*, 1997; Dobrianov *et al.*, 1999, 2001; Otalora *et al.*, 1999; Boggon *et al.*, 2000; Hu *et al.*, 2001; Vetter *et al.*, 2002). However, the topographic contrasts observed in protein crystals are poor compared with those in organic crystals of small molecules reported previously (Sherwood, 1990; Klapper, 1990, 1991). Thus, the interpretation of the topographic images in protein crystals is still controversial.

The most common contrast mechanism for the observation of crystal defects in X-ray topographs is the kinematical image (so-called direct image), produced by an additional diffracted intensity originating from distorted lattice areas close to each defect (Tanner, 1976; Klapper, 1991; Bowen & Tanner, 1998). The direct image can be obtained when $\mu t < 1$, where μ is the linear absorption coefficient and t is the thickness of the crystal. A further important criterion for the appearance of the direct image is that $t > \alpha\xi_g$, where ξ_g is the extinction distance and α is between 0.15 and 0.4 (Tanner, 1972). Generally, the extinction distance of protein crystals is much longer than for those of organic crystals of small molecules. Thus, the minimum criterion, $0.4\xi_g$, in the crystal thickness should be noted for X-ray topography of protein crystals where it is difficult to grow large crystals.

The topographic contrast of the direct image of a dislocation with Burgers vector **b** is proportional to a scalar product, $\mathbf{g}\cdot\mathbf{b}$, where **g** is the diffraction vector (Tanner, 1976; Klapper, 1991; Bowen & Tanner, 1998). Therefore, the dislocation imaged with reflection planes normal to **b**, *i.e.* with **g** parallel to **b**, generates a strong contrast, whereas, for reflection planes parallel to **b**, no contrast will appear. This means that the extinction of line contrasts in specific reflections is evidence for dislocation images. In addition, the most important character, *i.e.* the Burgers vector, of the dislocations can be experimentally determined from the extinction criterion of the dislocation images.

Protein crystals that include a large amount of water are very fragile. When protein crystals are exposed to air, water is easily evaporated so that strain and cracks are introduced into the crystals. In X-ray topography of protein crystals, the alignment of the crystal is troublesome, and rapid imaging is required. In the white-beam technique, *i.e.* the Laue method, alignment is not critical and the exposure is short, compared with the monochromatic beam technique. Moreover, in the Laue method, a number of reflections (topographs) can be recorded on one film by one exposure. This can make it easy to experimentally determine the Burgers vectors of the dislocations. Thus, white-beam topography appears to be a more suitable method for characterizing dislocations in protein crystals. In addition, the white beam from synchrotron radiation can provide extremely small beam divergence due to the high collimation of the white beam and the large distance between the source and the sample. This can achieve a good instrumental resolution in white-beam topography.

We have obtained tetragonal hen egg-white (HEW) lysozyme crystals up to a size of 4 mm by a salt concentration-gradient method. For the grown large protein crystals, X-ray topography was carried out using white-beam synchrotron radiation. Line contrasts clearly appeared on the Laue topographs. Moreover, the extinction of the line contrasts was observed in specific reflections. In this paper we report the identification of dislocations in tetragonal HEW lysozyme crystals by means of synchrotron white-beam topography.

2. Experimental

2.1. Crystal growth

Tetragonal HEW lysozyme crystals were grown by the salt concentration-gradient method suggested by Ataka & Katsura (1992). HEW lysozyme (crystallized six times, Seikagaku Kogyo, Japan) was dissolved in distilled water to 5%. The solution was adjusted to pH 4.5 using HCl. A $NiCl_2$ precipitant was put in the bottom of a vertically held test tube, to which the lysozyme solution was slowly added. The test tube was kept at 296 K in a clean room. The $NiCl_2$ naturally diffuses upwards so that a concentration gradient, *i.e.* solubility distribution, is formed along the tube. The solubility is a minimum at $\sim$8% $NiCl_2$ and around that point the crystallization occurs. The number of nuclei is limited so that only a few large crystals are grown. After two weeks, large crystals up to $\sim$4 mm were obtained in the solution (Tachibana *et al.*, 1999, 2000; Tachibana & Kojima, 2002). The crystals were tetragonal with space group $P4_32_12$, lattice constants of $a = b = 79.1$ Å, $c = 37.9$ Å, and eight molecules per unit cell. The crystals were bounded by the crystal-

lographic faces {110} and {101}. Crystals of thicknesses greater than 1.5 mm were selected for X-ray topographic experiments.

2.2. X-ray topography

X-ray topography was carried out using white-beam synchrotron radiation on BL15B1 at the Photon Factory (PF) of the High Energy Accelerator Research Organization (KEK) and on BL28B2 at SPring-8. Synchrotron white-beam topography on BL15B1 has been successfully used for a number of crystals of small organic molecules such as benzophenone, urea, *N*-methylurea and 2,3-dimethylnaphthalenene (Tachibana *et al.*, 1992, 1993, 1994, 1999; Shimizu *et al.*, 1997). The synchrotron white-beam topographic system for organic crystals has been installed on BL28B2 at SPring-8 (Chikaura *et al.*, 2001; Tachibana & Kojima, 2002).

The synchrotron white beam was strongly scattered in the test tube in which tetragonal HEW lysozyme crystals were grown. For synchrotron white-beam topography, the crystal in the test tube was gently transferred into a thin container, *e.g.* a short straw made of polypropylene, which was transparent to the synchrotron white beam. To avoid the evaporation of water contained in the crystal, it was surrounded by a growth solution and both ends of the straw were sealed with parafilm. The sealed straw was mounted on the goniometer, and the crystallographic direction [001] or [110] of the tetragonal HEW lysozyme crystal was adjusted to be almost parallel to the incident synchrotron white beam. The camera length was 25 cm. Topographs were recorded on X-ray films (AGFA D2) with exposure times of $\sim$10 s on BL15B1 at PF or of a few seconds on BL28B2 at SPring-8.

The high power of the synchrotron white beam gives rise to radiation damage. Most of the radiation damage is due to heating of the crystals by irradiating long wavelengths. To avoid this heating, metal plates are usually used as filters. However, the metal filters were not effective for protein crystals (Izumi *et al.*, 1996). We considered the possibility that radiation damage in protein crystals was due to the specific wavelengths absorbed by the water in the crystals. Water was then used as a filter. As a result, radiation damage was drastically reduced. The water filter was very effective in the synchrotron white-beam topography of protein crystals (Izumi *et al.*, 1999).

The synchrotron white-beam wavelength profile at the sample strongly depended on the thickness of the water filter. The synchrotron white-beam profile after filtration on BL15B1 at PF was calculated for water filters of different thicknesses. As shown in Fig. 1, the total intensity through a water filter of thickness 4 mm was reduced by an order of magnitude compared with that of the raw synchrotron white beam. This filtration mainly decreased the intensities with wavelengths longer than 1 Å. Consequently, the wavelength with the maximum intensity was shifted from 3.5 to 0.9 Å. The thicker 30 mm water filter led to a further shift of the maximum intensity wavelength to 0.6 Å, with additional reduction of the total intensity. As a result, even the intensities with wavelengths around 1 Å required for synchrotron white-beam topography were drastically decreased. For these calculations the water filter of thickness 4 mm was found to be more effective for synchrotron white-beam topography of the tetragonal HEW lysozyme crystals. The 4 mm water filter allowed acquisition of several successive topographs from the same crystal.

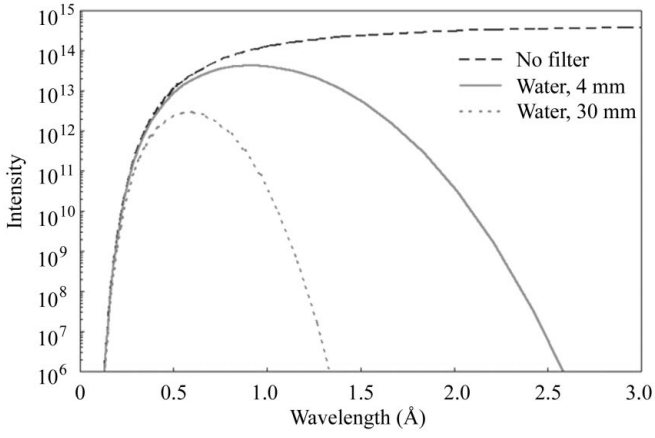

Figure 1
Synchrotron white-beam profiles with wavelength arriving at the sample on BL15B1 at PF. The effect on the white-beam spectrum of the filtrations through 4 mm and 30 mm of water is shown. The intensity scale is logarithmic.

3. Results and discussion

Fig. 2 shows a synchrotron Laue topographic pattern recorded with the incident white beam almost parallel to the [001] crystallographic direction of the tetragonal HEW lysozyme crystal on BL15B1 at PF. The Laue pattern was analysed using a Laue analytical program developed by Norm Engineering. As a result, the observed Laue pattern was found to be recorded with the incident white beam tilted by 6° to the [001] direction of the tetragonal HEW lysozyme crystal. Each Laue spot (topograph) includes higher-order crystallographic reflections with higher harmonic wavelengths. The lowest-order reflections are indicated for intense Laue topographs of interest in Fig. 2. For example, the Laue topograph labeled 200 in Fig. 2 contains 400, 600 and 800 reflections and so on.

Laue topographs of crystals with larger lattice constants such as protein crystals include more harmonic reflections. The broader the white-beam spectrum, the more harmonics that may simultaneously satisfy Bragg's law will contribute to the topograph. The predominant harmonic component of the Laue topograph should be identified for the analysis of topographic images. The relative contributions of the series of harmonic reflections can be calculated using beam-profile intensities, theoretical relationships derived for perfect crystals, and

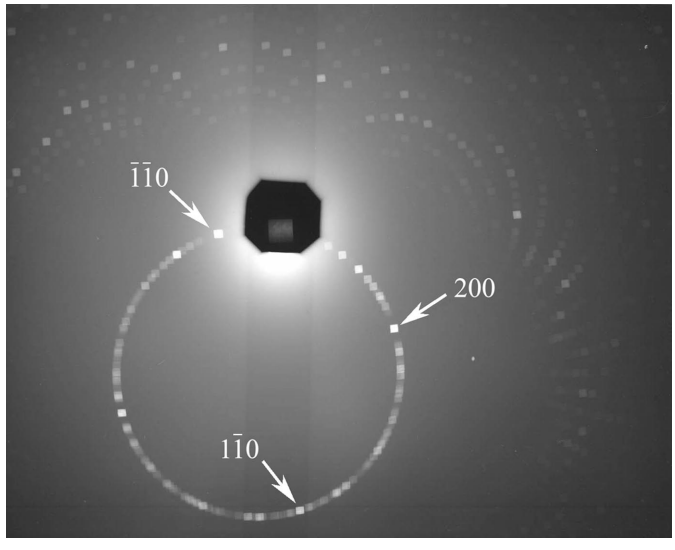

Figure 2
Laue topographic pattern recorded with the synchrotron white beam almost parallel to [001] of the tetragonal HEW lysozyme crystal.

Table 1
Calculated relative intensities I_h contributed by higher-order reflections in the Laue topograph labeled 200 in Fig. 2.

$P(\lambda)$ is the relative distribution of X-ray intensity of wavelength λ arriving at the sample after the 4 mm water filtration on BL15B1 of PF (Fig. 1), F_{hkl} is the structure factor for the reflection, θ is the Bragg angle, μ is the linear absorption coefficient and t is the thickness of the crystal used. Here, the absorption has been described roughly by the factor $\exp(-\mu t)$. The values of $|F_{hkl}|$ were taken from experimental data.

Reflection	θ (°)	λ (Å)	$\lvert F_{hkl}\rvert$	$P(\lambda)$	$\exp(-\mu t)$	I_h
200	3.25	4.48	575	$<10^{-3}$	1.03×10^{-5}	$<10^3$
400	3.25	2.24	885	2.30×10^{-3}	0.22	1.5×10^3
600	3.25	1.49	41	13	0.62	3.6×10^5
800	3.25	1.21	695	70	0.81	1.7×10^7
10,0,0	3.25	0.89	649	90	0.90	1.1×10^7
12,0,0	3.25	0.74	338	73	0.94	3.0×10^6
14,0,0	3.25	0.64	186	49	0.96	7.2×10^5

absorption (Tuomi *et al.*, 1974). The relative diffracted intensities, I_h, contributed by the harmonics were obtained using the following equation,

$$I_h = P(\lambda)|F_{hkl}|\lambda^3 \operatorname{cosec}^2\theta \exp(-\mu t), \quad (1)$$

where $P(\lambda)$ is the relative distribution of X-ray intensity of wavelength λ arriving at the sample after the 4 mm water filtration on BL15B1 at PF (Fig. 1), F_{hkl} is the structure factor for the reflection, θ is the Bragg angle, μ is the linear absorption coefficient and t is the thickness of the crystal. Here, the absorption has been described roughly by the factor $\exp(-\mu t)$. The relative diffracted intensities contributed by the harmonics were calculated for intense Laue topographs labeled 200, $\bar{1}\bar{1}0$ and $1\bar{1}0$ in Fig. 2. For example, the relative contributions of higher-order reflections in the Laue topograph labeled 200 are presented in Table 1. The predominant component contributing to the 200 Laue topograph is found to be the 800 reflection as presented in Table 1. Similar calculations were also carried out for other Laue topographs labeled $\bar{1}\bar{1}0$ and $1\bar{1}0$ in Fig. 2. The predominant components contributing to the $\bar{1}\bar{1}0$ and $1\bar{1}0$ Laue topographs were found to be the $\bar{4}\bar{4}0$ and $12,\bar{1}\bar{2},0$ reflections, respectively.

The minimum criterion, $0.4\xi_g$, in the crystal thickness for the visibility of direct images in X-ray topographs was calculated for the 800, $\bar{4}\bar{4}0$ and $12,\bar{1}\bar{2},0$ reflections indexed above. The extinction distance, ξ_g, for a symmetrical reflection in a perfect crystal (Tuomi *et al.*, 1974; Tanner, 1976; Bowen & Tanner, 1998) is given by

$$\xi_g = (\pi/r_e)V_c \cos\theta/|F_{hkl}|\lambda, \quad (2)$$

where r_e is the classical electron radius and V_c is the unit-cell volume. The dominant factor determining the extinction distance of a given reflection is the ratio of the cell volume to its structure amplitude. Therefore, the extinction distances in common protein crystals with larger unit-cell volumes are much larger than those for crystals of small organic molecules and are sometimes as much as an order of magnitude longer than dimensions of the protein crystals available. The minimum criterion, $0.4\xi_g$, in crystal thickness for the visibility of direct images should be a particular concern, especially where it is difficult to grow large protein crystals. The values of the minimum criterion, $0.4\xi_g$, in the crystal thickness calculated for the 800, $\bar{4}\bar{4}0$ and $12,\bar{1}\bar{2},0$ reflections are presented in Table 2. The calculated values are 1.35, 1.11 and 1.42 mm for the 800, $\bar{4}\bar{4}0$ and $12,\bar{1}\bar{2},0$ reflections, respectively. These values are much larger than the dimensions of protein crystals so far studied by X-ray topography (Izumi *et al.*, 1996, 1999; Stojanoff & Siddons, 1996; Stojanoff *et al.*, 1997; Dobrianov *et al.*, 1999, 2001; Otalora *et al.*, 1999; Boggon *et al.*, 2000; Hu *et al.*, 2001; Vetter *et al.*, 2002). This means that it was difficult to obtain a direct image of the previous protein crystals. The tetragonal HEW lysozyme crystals used in this work were more than 1.5 mm in thickness, which is large compared with the calculated values of $0.4\xi_g$ for all of the reflections indexed above. Thus, it is expected that a sufficient contrast of crystal defects, especially dislocations, in the topographs can be obtained from the large crystals used in this work.

Table 2
The minimum criterion, $0.4\xi_g$, in the sample thickness for the appearance of the direct images for Laue topographs in the 800, $\bar{4}\bar{4}0$ and $12,\bar{1}\bar{2},0$ reflections, where ξ_g is the extinction distance.

Reflection	$0.4\xi_g$ (mm)
800	1.35
$\bar{4}\bar{4}0$	1.11
$12,\bar{1}\bar{2},0$	1.42

Figs. 3(*a*), 3(*b*) and 3(*c*) show enlarged photographs of the Laue intensities labeled 200, $\bar{1}\bar{1}0$ and $1\bar{1}0$ in Fig. 2, respectively, which correspond to Laue topographs with predominant harmonic reflections of 800, $\bar{4}\bar{4}0$ and $12,\bar{1}\bar{2},0$ indexed as above. As seen in Fig. 3(*a*), straight lines from the core of the crystal are clearly observed. They are almost parallel to the $[1\bar{1}0]$ or [110] crystallographic directions. The distribution of the lines is similar to that of grown-in dislocations commonly observed in solution-grown crystals (Klapper, 1991). The lines parallel to $[1\bar{1}0]$ are invisible in the $\bar{4}\bar{4}0$ reflection in Fig. 3(*b*), and those parallel to [110] are invisible in the $12,\bar{1}\bar{2},0$ reflection in Fig. 3(*c*). Such extinction of the line images means that they are dislocation images. According to the invisibility criterion ($\mathbf{g}\cdot\mathbf{b} = 0$) of the dislocation images, the Burgers vectors are determined to be $[1\bar{1}0]$ and [110] for the dislocations parallel to $[1\bar{1}0]$ and [110], respectively. The directions of the Burgers vectors are coincident with those of the corresponding dislocations. Therefore, it is concluded that the predominant dislocations in tetragonal HEW lysozyme crystals are of screw character with $\langle 110\rangle$ Burgers vectors. In addition, from the topographs in Fig. 3, the density of dislocations in the crystal is estimated to be $\sim 2.7 \times 10^2$ cm^{-2}.

To clarify the origin of the observed $\langle 110\rangle$ dislocations, it is worthwhile to consider all possible Burgers vectors in tetragonal HEW lysozyme crystals. According to dislocation theory (Hirth & Lothe, 1982), the dislocation energy E per unit length of a straight dislocation consists of two terms. One is the elastic energy E_a due to the long-range strain field surrounding a dislocation. The other is the dislocation core energy E_c. However, E_c can be neglected without serious error, since it is usually estimated to be at least one order of magnitude smaller than E_a. Thus, E is approximately given by E_a, *i.e.*

$$E \simeq E_a = \left(G\mathbf{b}^2/4\pi\right)\ln(R/r_0), \quad (3)$$

where G is the shear modulus and R and r_0 are the outer and inner cut-off radii of the dislocation concerned. The shear modulus G was estimated from the sound velocity measured previously (Tachibana *et al.*, 2000, 2002). Equation (3) shows that the dislocation energy is proportional to the square of the magnitude of the Burgers vector (Kojima, 1991). This implies that the shorter lattice translational vectors are favored as Burgers vectors. The possible Burgers vectors in tetragonal HEW lysozyme crystals are listed in Table 3. A perfect dislocation with Burgers vector [110] can be dissociated into two partial dislocations, $\frac{1}{2}[110] + \frac{1}{2}[110]$, since they reduce the elastic energy of the dislocation.

The predominant Burgers vector $\langle 110\rangle$ observed in this work is not the shortest of possible Burgers vectors in Table 3. Such long Burgers

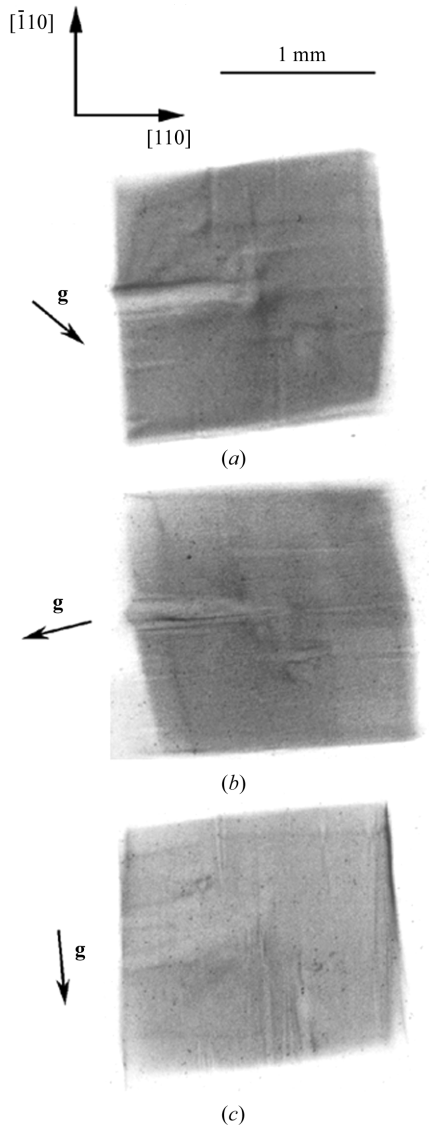

Figure 3
Laue topographs of (*a*) 800, (*b*) $\bar{4}\bar{4}0$ and (*c*) $12,1\bar{2},0$ reflections, respectively, enlarged from the Laue intensities labeled 200, $1\bar{1}0$ and $1\bar{1}0$ in Fig. 2.

Table 3
Possible Burgers vectors **b** of dislocations in tetragonal HEW lysozyme crystals.

$G\mathbf{b}^2$ is also given in this table, since the dislocation energy is proportional to $G\mathbf{b}^2$ as shown in equation (3), where G is the shear modulus estimated from the sound velocity measured previously (Tachibana *et al.*, 2000, 2002).

b	$\lvert\mathbf{b}\rvert$ (Å)	G (GPa)	$G\mathbf{b}^2$ (10^{-10} J m^{-1})
[001]	37.9	1.02	147
[100]	79.1	1.02	638
[010]	79.1	1.02	638
[101]	87.7	1.02	785
[110]	111.8	1.02	1275
$\frac{1}{2}$[110]	55.9†	1.02	637‡

† Magnitude of the Burgers vector of the partical dislocation $\frac{1}{2}$[110]. ‡ Sum of the values of $G\mathbf{b}^2$ for two partial dislocations.

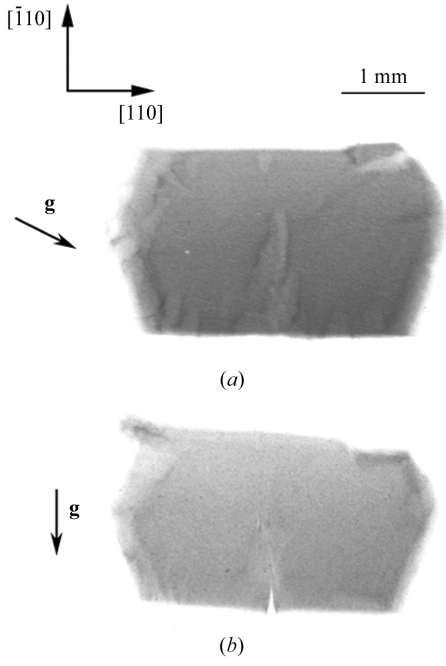

Figure 4
Laue topographs of (*a*) $1\bar{1}\bar{2}$ and (*b*) $12,\bar{1}\bar{2},0$ reflections recorded with the synchrotron white beam almost parallel to [110] in the tetragonal HEW lysozyme crystal including cracks.

vectors, however, have often been observed, especially during the growth of organic crystals (Izumi, 1996; Shimizu *et al.*, 1997). In fact, the ⟨110⟩ spiral growth in tetragonal HEW lysozyme crystals has been observed by means of AFM (Durbin *et al.*, 1993; Konnert *et al.*, 1994; Malkin *et al.*, 1999; McPherson *et al.*, 2001). Thus, the observed ⟨110⟩ screw dislocation corresponds to the preferential ⟨110⟩ spiral growth in tetragonal HEW lysozyme crystals.

Another Burgers vector was also observed in a tetragonal HEW lysozyme crystal containing cracks. Figs. 4(*a*) and 4(*b*) show Laue topographs recorded with the incident white beam almost perpendicular to the [110] direction of the crystal. The cracks in the crystal were observed on the topographs with all reflections. The direction of the crack is perpendicular to [001]. It should be noticed that loop lines were clearly observed around the cracks as shown in Fig. 4(*a*). The loop lines are visible with the $1\bar{1}\bar{2}$ refection in Fig. 4(*a*) and invisible with the $12,\bar{1}\bar{2},0$ reflection in Fig. 4(*b*). This extinction of the line images means that they are dislocation images. From the extinction criterion of the dislocation images, the Burgers vector can be determined to be [001], which is the shortest of possible Burgers vectors in tetragonal HEW lysozyme crystals, as presented in Table 3.

In general, slip dislocations introduced by slippage have the shortest Burgers vectors. The slips, *i.e.* slip lines, in tetragonal HEW lysozyme crystals have been previously observed by indentation (Tachibana *et al.*, 1999). Therefore, the slip can also occur by stress concentration during the formation of cracks. This suggests that the observed dislocation loops are slip dislocations produced by stress concentration. According to a previous report (Tachibana *et al.*, 1999), the most densely packed plane is (110). Therefore, the slip plane is likely to be (110). The (110) plane contains the shortest Burgers vector [001]. This suggests that (110)[001] is the most probable slip system. Thus, the observed [001] dislocation loops would be introduced by the operation of the (110)[001] slip system in tetragonal HEW lysozyme crystals.

We would like to thank Dr M. Ataka of the National Institute of Advanced Industrial Science and Technology (AIST) for his helpful information on the crystal growth of tetragonal HEW lysozyme crystals. We also thank Dr H. Sugiyama of the Institute of Materials Structure Science for his help on the experimental set up in BL15B1 at PF. The synchrotron radiation experiments were performed at the Photon Factory under the auspices of the Photon Factory Program Advisory Committee of the High Energy Accelerator Research Organization (KEK) (Proposal Nos. 2001G062, 2003G022) and at SPring-8 with the approval of the Japan Synchrotron Radiation Research Institute (JASRI) (Proposal No. 2001A0220-ND-np, 2001B0200-ND-np, 2002A0523-ND3-np, 2002B0543-ND3-np, 2003A0225-ND3-np).

References

Ataka, M. & Katsura, T. (1992). *The 4th International Conference on Biophysics and Synchrotron Radiation*, Tsukuba, Japan. Abstracts, p. 354.
Boggon, T. J., Helliwell, J. R., Judge, R. A., Olczak, A., Siddons, D. P., Snell, E. H. & Stojanoff, V. (2000). *Acta Cryst.* D**56**, 868–880.
Bowen, D. K. & Tanner, B. K. (1998). *High-Resolution X-ray Diffractometry and Topography*. London: Taylor and Francis.
Chikaura, Y., Iida, S., Kawado, S., Kimura, S., Matsui, J., Umeno, M., Ozaki, T., Shimura, T., Suzuki, Y., Izumi, K., Kawasaki, K. & Ishikawa, T. (2001). *J. Phys. D*, **34**, A158–A162.
Dobrianov, I., Caylor, C., Lemay, S. G., Finkelstein, K. D. & Thorne, R. E. (1999). *J. Cryst. Growth*, **196**, 511–523.
Dobrianov, I., Kriminski, K., Caylor, C. L., Lemay, S. G., Kimmer, C., Kisseley, A., Finkelstein, K. D. & Thorne, R. E. (2001). *Acta Cryst.* D**57**, 61–68.
Durbin, S. D., Carlson, W. E. & Saros, M. T. (1993). *J. Phys. D*, **26**, B128–B132.
Hirth, J. P. & Lothe, J. (1982). *Theory of Dislocations*, 2nd ed. New York: Wiley.
Hu, Z. W., Lai, B., Chu, Y. S., Cai, Z., Mancini, D. C., Thomas, B. R. & Chernov, A. A. (2001). *Phys. Rev. Lett.* **87**, 148101-1–148101-4.
Izumi, K. (1996). *J. Cryst. Growth*, **169**, 325–330.
Izumi, K., Sawamura, S. & Ataka, M. (1996). *J. Cryst. Growth*, **168**, 106–111.
Izumi, K., Taguchi, K., Kobayashi, Y., Tachibana, M., Kojima, K. & Ataka, M. (1999). *J. Cryst. Growth*, **206**, 155–158.
Klapper, H. (1990). *Defect Control in Semiconductors*, edited by K. Sumino, pp. 1641–1652. Amsterdam: North-Holland.
Klapper, H. (1991). *Crystals*, Vol. 13, edited by H. C. Freyhardt, pp. 109–162. Berlin: Springer.
Kojima, K. (1991). *Progress in Crystal Growth and Characterization*, edited by N. Niizeki, pp. 369–420. Oxford: Pergamon.
Konnert, J. H., D'Antonio, P. & Ward, K. B. (1994). *Acta Cryst.* D**50**, 603–613.
McPherson, A., Malkin, A. J., Kuznetsov, Yu. G. & Plomp, M. (2001). *Acta Cryst.* D**57**, 1053–1060.
Malkin, A. J., Kuznetsov, Yu. G. & McPherson, A. (1999). *J. Cryst. Growth*, **196**, 471–488.
Otalora, F., Garcia-Ruiz, J. M., Gavira, J. A. & Capelle, B. (1999). *J. Cryst. Growth*, **196**, 546–558.
Sherwood, J. N. (1990). *Defect Control in Semiconductors*, edited by K. Sumino, pp. 1611–1621. Amsterdam: North-Holland.
Shimizu, M., Tachibana, M., Inoue, K. & Kojima, K. (1997). *J. Cryst. Growth*, **177**, 135–139.
Stojanoff, V. & Siddons, D. P. (1996). *Acta Cryst.* A**52**, 498–499.
Stojanoff, V., Siddons, D. P., Monaco, L. A., Vekilov, P. & Rosenberger, F. (1997). *Acta Cryst.* D**53**, 588–595.
Tachibana, M., Horiuchi, S., Wang, J. S. & Kojima, K. (1993). *J. Phys. D*, **26**, B145–B148.
Tachibana, M., Kobayashi, Y., Shimazu, T., Ataka, M. & Kojima, K. (1999). *J. Cryst. Growth*, **198/199**, 661–664.
Tachibana, M. & Kojima, K. (2002). *Curr. Top. Cryst. Growth Res.* **6**, 35–49.
Tachibana, M., Kojima, K., Ikuyama, R., Kobayashi, Y. & Ataka, M. (2000). *Chem. Phys. Lett.* **332**, 259–264.
Tachibana, M., Kojima, K., Ikuyama, R., Kobayashi, Y. & Ataka, M. (2002). *Chem. Phys. Lett.* **354**, 360.
Tachibana, M., Kono, K., Shimizu, M. & Kojima, K. (1999). *J. Cryst. Growth*, **198/199**, 665–669.
Tachibana, M., Motomura, S., Uedono, A., Tang, Q. & Kojima, K. (1992). *Jpn. J. Appl. Phys.* **31**, 2202–2205.
Tachibana, M., Tang, Q., Ide, N. & Kojima, K. (1994). *Jpn. J. Appl. Phys.* **33**, 1995–2003.
Tanner, B. K. (1972). *Phys. Status Solidi A*, **10**, 381–386.
Tanner, B. K. (1976). *X-ray Diffraction Topography*. Oxford: Pergamon.
Tuomi, T., Naukkarinen, K. & Rabe, P. (1974). *Phys. Status Solidi A*, **25**, 93–106.
Vetter, W. M., Gallagher, D. T. & Dudley, M. (2002). *Acta Cryst.* D**58**, 579–584.